CHAPTER 5

Nanomaterials for Energy Conversion Applications

V. Renugopalakrishnan,[1,2] A. M. Kannan,[3] S. Srinivasan,[4] V. Thavasi,[5] S. Ramakrishna,[5] P. Li,[1] A. Mershin,[6] S. Filipek,[7] A. Kumar,[5] J. Dutta,[8] A. Jaya,[9] L. Munukutla,[3] S. Velumani,[10] G. F. Audette[11]

[1]*Children's Hospital, Harvard Medical School, Boston, MA 02115, USA*
[2]*Department of Chemistry and Chemical Biology, Northeastern University, Boston, MA 02115, USA*
[3]*Electronic Systems Department, Arizona State University, Mesa, AZ 85212, USA*
[4]*Clean Energy Research Center, University of South Florida, Tampa, FL 33620, USA*
[5]*NUS Nanotechnology Initiative (NUSNNI), National University of Singapore, Singapore-117576*
[6]*Center for Biomedical Engineering, Massachusetts Institute of Technology, Cambridge, MA 02139, USA*
[7]*International Institute of Molecular and Cell Biology, 02-109 Warsaw, Poland*
[8]*Center for Excellence in Nanotechnology, School of Engineering & Technology, Asian Institute of Technology, Pathumthani 12120, Thailand*
[9]*Dr. A.L. Mudaliar Post Graduate Institute of Basic Medical Sciences, University of Madras, Taramani Campus, Chennai – 600 113, India*
[10]*Department of Physics, Tecnológico de Monterrey, Av. E. Garza Sada 2501, Monterrey, N. L., Mexico*
[11]*Department of Chemistry, York University, Toronto, ON, M3J1P3, Canada*

CONTENTS

ISBN: 1-58883-120-5

Nanomaterials for Energy Storage Applications
Edited by Hari Singh Nalwa
Pages: 155–178

1. INTRODUCTION

Nanostructured materials are gaining importance for energy creation and storage. In this chapter, we focus on protein-based and inorganic nanostructured materials in harnessing solar energy and creation of electrical energy. This chapter addresses recent research in protein-sensitized wide gap semiconductor-based solar cells, protein-based fuel cells, and hydrogen storage by nanomaterials. Bionanostructured materials are unique in their design and can be tailored with the use of biotechnology. In the case of biosolar and biofuel cells, the proteins can be designed by rational site-directed protein engineering by fine tuning their band gaps and by increasing the rate of electron transfer by altering the amino acid residues surrounding the metal coordination center, e.g., in blue copper-containing azurins, heme-containing Cytochrome c superfamily. Hybrid bioinorganic systems seem promising in energy generation, conversion, and storage applications.

2. BIOSOLAR CELL

Photovoltaics (PVs) essentially consist of solar cells fabricated from semiconductors that convert energy from sunlight into electrical power. Therefore, potentially they are one of the most important renewable energy sources. Existing crystalline silicon solar cell technologies involve high material costs and face a severe shortage of raw wafers. Consequently, although the "fuel" for a solar-powered generator is sunlight, which is "free," the overall cost of solar-generated electricity is still much greater than the cost of electricity generated by burning fossil fuels or through nuclear reactors. The silicon solar cells widely used for terrestrial applications have the greatest efficiency (defined as the electrical energy produced for a given input of solar energy). However, over the years, despite the introduction of thin film technologies, neither greater efficiency nor reduced manufacturing cost of solar cells could be achieved for wider acceptance in terrestrial power generation.

Chlorophyll a and b, bacteriochlorophyll, Photosystems I and II, and bacteriorhodopsin (bR) mutants exhibit a wide range of light absorption in their spectrum where they can be excited, and they can be spectrally fine-tuned by the use of biotechnology. bR manifests high quantum efficiency and thermal robustness, which are mandatory requirements for biosensitized solar cells (BSSCs) to function in daylight, where temperatures may surpass 100°C. The low cost of producing bR mutants and their lack of toxicity are two key assets that the ruthenium (Ru) dye lacks at the present time. BSSC shows promise in the harnessing of the sun's energy and has exciting commercial prospects. The most important attributes of this project, distinct from dye-sensitized solar cells (DSSCs), are (1) the replacement of the Ru dye in a DSSC by environmentally friendly light-harvesting proteins, (2) the use of nanofibers and nanowires for increased surface area on the semiconductor layers for enhanced efficiency of the complete device, and (3) the use of low-cost metallization techniques for the fabrication of cost-effective, stable solar modules. Most of the proposed fabrication principle consists of aqueous media and operates at low temperatures, which renders the process environmentally friendly. A number of previous reports on biosolar cells have appeared in the literature [1–8].

The photoelectrochemical cell developed by Gratzel is biomimetic in nature and is an example of nanoscale engineering par excellence, but it does not contain any biologically derived material. The practical technological application of photosynthesis based on semiconductor-driven coupled redox reactions (photo-oxidation and photoreduction) could be a better alternative for photovoltaic energy generation. In such devices, the electron-hole pairs formed by absorption of a photon, instead of being used to drive electric current, are used as chemically active agents to drive coupled redox reactions. The hole is a strong oxidizing agent, whereas the electron is a strong reducing agent, and they can bring about reactions that are energetically uphill.

Light-harvesting proteins contain properties that might form the basis of a new kind of solar cell capable of converting light energy to usable forms of chemical energy. Among the light-harvesting proteins, bR occupies an important role because it has been widely investigated in many laboratories, including ours. An attractive feature is that bR is produced by *Halobacterium salinarum* as monolayer crystalline chips of submicron dimensions. The present research on BSSCs in different laboratories is being directed toward using genetically altered variants of bR to replace Ru dye, the black dye tri(cyanato)-2,2′,2″-tetrapyridyl-4,4′,4″-tricarboxylate Ru(II), which is the major electron donor in DSSCs. DSSCs were developed by Gratzel's group, the Ecole Polytechnique Federale de Lausanne [9–11].

The DSSC is based on the concept of charge separation at an interface of two materials of a different conduction mechanism and the matching of energy band gaps. Until recently, solar cells have been dominated by inorganic solid-state devices, such as silicon. The DSSC was the first attempt to sensitize nanocrystalline and conducting polymers with the Ru dye. Sensitizing dyes used for solar cell applications include, for instance, 4,4′,4″,4‴−(21*H*-23*H*-porphine-5,10,15,20-tetrayl)tetrakis (benzoic acid) (TPPAc), *cis*di(thiocyanato)-*N,N*-bis(2,2′-bipyridyldicarboxylate)-ruthenium(II) (N3), and (tri(cyanato)2,2′,2″-terpyridyl-4,4′,4″-tricarboxylate)ruthenium(II) (black dye). Contrary to expectations, solar cells based on interpenetrating networks of mesoscopic semiconductors sensitized by dyes have shown greater photochemical conversion efficiencies. A typical prototype of DSSC leverages on the optical absorption and the charge separation processes by the association of a sensitizer as the light-absorbing material in conjunction with a wide band-gap semiconductor such as nanocrystalline TiO_2. DSSC contains a mesoporous oxide layer composed of nanometer-sized particles sintered together to allow for electron conduction to occur. TiO_2, SnO_2, ZnO, and Nb_2O_3 nanofibers and wires have been the choice of semiconductor in the construction of DSSCs. A charge transfer or relay dye is attached either covalently or by the process of chemisorption to the nanocrystalline oxide film. Photoexcitation of the dye results in the injection of an electron into the conduction band of the oxide. The original state of the dye is subsequently reset by electron donation from the electrolyte, usually an organic solvent containing a redox system, for instance, iodide/triiodide couple. The regeneration of the sensitizer, the Ru dye, intercepts the recapture of the conduction band electron by the oxidized dye. The iodide is regenerated in turn by the reduction of triiodide at the counter electrode, the circuit being completed via electron migration through the external load. The voltage generated under illumination from a Xe lamp in the laboratory or sun light in actual operating condition is the difference between the Fermi level of the electron in the solid state and the redox potential of the electrolyte.

On the basis of the aforementioned advantages of light-harvesting proteins over Ru dye and the great need for ordered metal-oxide electrodes in DSSC, we have a reasonable expectation that collection of solar cells composed of ordered metal oxide, such as ZnO nanowires and TiO_2

nanofibers, sensitized by light-harvesting proteins, will surpass the efficiency of existing Ru dye-sensitized solar cells. The innovations that make the biosolar cell stand apart are (1) their light-harvesting proteins with faster electron ejection rates, high quantum efficiency, broad-band absorption including near the IR region, thermal robustness, and nontoxicity offer unsurpassable superiority to the Ru dye and (2) ordered one-dimensional wide-gap semiconductors, such as nanofibers and nanowires which are better for collecting and transporting electrons, are vastly superior to TiO_2 nanoparticles. Despite these sterling advantages, we need to develop methods to couple proteins to TiO_2 and ZnO surfaces and explore less toxic, less-corrosive and nonvolatile electrolytes. Our hypothesis, stated in a nut-shell, is that the fast electron ejection rate of light-harvesting proteins coupled to TiO_2 nanofibers and ZnO nanowires affords significant advantages to Ru dye-sensitized TiO_2 solar cells.

With the phenomenal development of protein science, there are number of potential candidates as sensitizers, out of which bacteriorhodopsin and Photosystem I and II prove to be the most promising. Similarly, in case of metal oxide electrodes, the TiO_2 nanofibers and ZnO nanowires had been chosen as model electrode to test the validity of our hypothesis. The advantages of the respective protein and metal oxides, with the scientific reasons for their selection, are discussed in Sections 3 and 4.

3. BACTERIORHODOPSIN: A UNIQUE ENERGY TRANSDUCER

bR acts as a proton "pump" in a "battery" that dissociates water into hydrogen and oxygen. An attractive feature is that bR is produced by *Halobacterium salinarum* as monolayer crystalline chips of submicron dimensions. Purple membrane patches (Figure 1), occur in a form that gives it rigidity and makes it feasible for incorporation in a physical device designed to capture sunlight. Seven transmembrane alpha-helices that belong to the G-coupled protein receptor family constitute the basic structural motif of bR (Figure 2). When bR absorbs light, it undergoes a series of structural changes accompanied by alteration in absorption spectrum (i.e., color) and refractive index of the protein (Figure 2). During this process, a positive charge is transferred from the inner to the outer side of the cell, which is the basis for the subsequent energy storage/generation process the bacterium [12].

To realize the full potential of bR-based BSSC, the choice of the right bR mutant as a replacement for the Ru dye in a DSSC is crucial. In general, mutants that manifest thermal stability and high quantum efficiency are ideal candidates for incorporation into the existing architecture of DSSC to replace Ru.

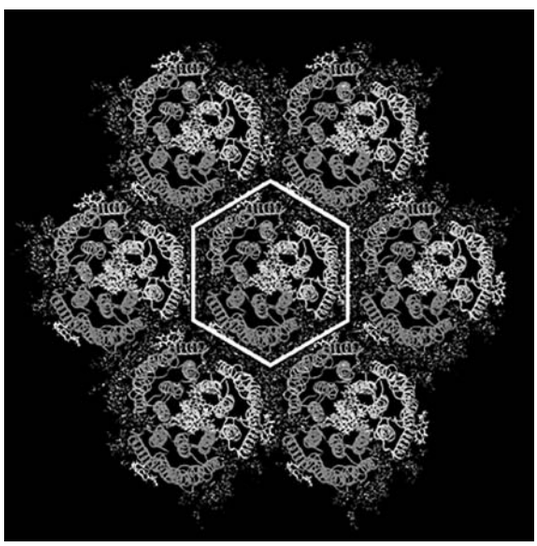

Figure 1. Purple membrane patches. Reprinted with permission from [12], V. Renugopalakrishnan et al., *IEEE Trans. Magnetics* 43, 773 (2007). © 2007, IEEE.

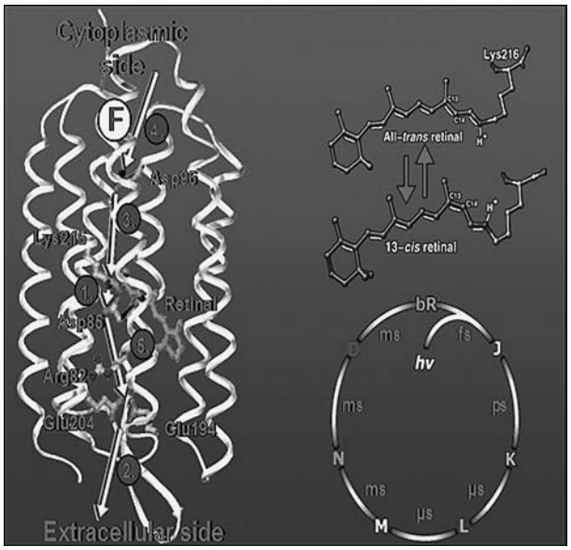

Figure 2. Structure of bR and photochemical cycle of bR. Reprinted with permission from [12], V. Renugopalakrishnan et al., *IEEE Trans. Magnetics* 43, 773 (2007). © 2007, IEEE.

4. LIGHT-ACTIVATED PROTEIN-SENSITIZED SOLAR CELLS

There have been reports in the literature leveraging light-harvesting proteins as sensitizers in photovoltaic cells, bR [1, 3–8, 14–24]. Photosynthetic reaction center based photovoltaic cell was reported by Lu [25]. Photoelectric differential response of bR-based photocell has been reported by Yao [2]. Oriented bR films were deposited on indium-tin oxide (ITO)-conductive glass by electrophoretic sedimentation and as Langmuir-Blodgett (LB) film. The bR film photocell was constructed as a sandwich-type electrochemical cell comprising junctions of ITO/bR/electrolyte/counterelectrode. Recent studies by Wang et al. [13] have demonstrated that dried bR film can be used in simple highly sensitive photodetector designs. Li et al. [20] have measured the photovoltage generated in an ITO detector by introducing polarization sensitivity through a photochemical bleaching process. Bertoncello et al. [4] have reported on the photovoltaic performance of bR LB films and compared them with organic and inorganic nanostructured solar materials and concluded significant increases in performance.

Xu et al. have measured photo-induced anisotropic photoelectric response in oriented bR films and its relevance to construction of bR based bio-photoreceiver. Electrical signals of light excited [D96N] bR were measured by Toth-Boconadi et al. Choi et al. studied the photoelectric response of bR adsorbed to self-assembled monolayers of 11-mercaptodecanoic acid on Au substrate as a template [5]. Manoj and Narayan [14] studied the opto-electrical processes at a conducting polymer-bR interface. Kay and Gratzel [23] reported the first set of experiments on photosensitization of TiO_2 solar cells by using chlorophyll derivatives and related naturally occurring porphyrins.

The aforementioned authors [23] measured an open circuit photovoltage of 0.52 V and a short circuit current density of 9.4 mA/cm^2 under simulated sunlight illumination. The overall energy conversion efficiency of the solar cell was in part limited by ohmic losses at such high current densities. The mechanism of photosensitization of nanocrystalline TiO_2 solar cells was deduced from static and time-resolved fluorescence quenching and laser photolysis by Kay et al. [24].

5. LIGHT-ACTIVATED PROTEIN MANIFESTS BROAD-BAND ABSORPTION

Dye-sensitized TiO_2 and SiO_2 solar cells and Gratzel cells are of increasing interest to consumers because of a strong desire to increase the use of alternative energy sources besides fossil fuels. These particular solar cells are currently in use, but better efficiency is desired. Improving the absorption properties of the dyes by designing ones that can absorb strongly and continuously across the visible extending into the NIR region is one step that can be taken to obtain better efficiency.

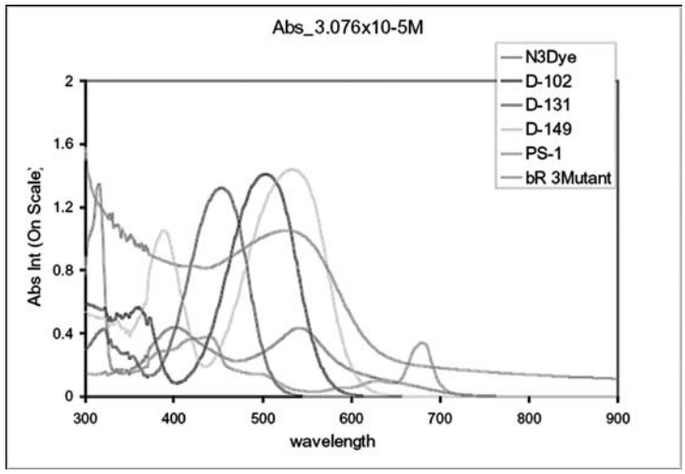

Figure 3. Absorption spectra of various proteins.

bR manifests absorption maxima, ranging from blue to red region of the visible spectrum. Hence, it is excitable in sunlight. Figure 3 compares the absorption spectra of bacteriorhodopsin triple mutant, [E9Q/E194Q/E204Q] bR, with photosystem I and Ruthenium dyes used in Gratzel's DSSC. The light-harvesting organic molecules and proteins manifest absorption maxima ranging from violet to near-IR regions and, hence, can be harnessed to capture the entire span of visible sun light.

5.1. Spectral Fine Tuning to Modulate the Absorption Characteristics of bR by Rational Protein Engineering

The absorption characteristics of light-activated proteins can be manipulated by the use of rational protein engineering. Much of the work reported in the literature has focused on sensory rhodopsins.

6. QUANTUM EFFICIENCY OF LIGHT-HARVESTING PROTEINS AND THEIR ENHANCEMENT BY RATIONAL PROTEIN ENGINEERING

One of the most important parameters when studying the performance of solar cells is the quantum efficiency. The quantum efficiency generally is defined as the ratio of the number of collected charge carriers to the number of incident photons at the device, and is named external quantum efficiency (EQE). Values in the literature for the quantum efficiency of the photochemical cycle of bR range from 0.25 to 0.79, and the sum of the quantum yields of the forward and back photoreactions been proposed to be 1 [25].

On the basis of the quantum yield of the photobleaching of rhodopsin, 0.67, the quantum efficiency of bR photoconversion was determined to be 0.64 ± 0.04. The quantum yield of M formation was found to be 0.65 ± 0.06. From the transient bleaching of bR at 610 nm with a saturating laser flash (28 mJ/cm^2), the maximum amount of bR cycling was estimated to be $47 \pm 3\%$. The ratio of the efficiencies of the forward and back light reactions, $[UNK]_1/[UNK]_2$, was estimated to be 0.67 ± 0.06 and, therefore, $[UNK]_2 \approx 1$ (0.94 ± 0.06). The sum of $[UNK]_1 + [UNK]_2 \approx 1.6$. It was found that repeated high-intensity laser flashes (>20 mJ/cm^2) irreversibly transformed bR into two stable photoproducts. One has its absorption maximum at 605 nm and the other has a well-resolved vibronic spectrum with maxima at 342, 359 (main peak), and 379 nm. We are investigating the quantum efficiencies of several light activated proteins using laser flash photolysis in collaboration with the University of Lund, Lund, Sweden.

7. QUANTUM EFFICIENCY OF RUTHENIUM DYE

Bauer et al. [26] have reported a quantum efficiency of 0.65 at 530 nm for Ru dye sensitized by SnO_2 which is surpassed by bR and its mutants. Therefore, bR can in principle compete and excel Ru dye.

8. MATCHING OF ENERGY BAND GAPS OF SEMICONDUCTORS: ELECTRON ACCEPTORS AND ELECTRON DONORS, Ru DYE, AND LIGHT-ACTIVATED PROTEINS

Preliminary studies indicate that there is a matching of the energy band gaps of bR and wide gap semiconductors. Estimation of energy band gaps of bR mutants with the use of the density functional theory calculations are impossible given the size of the protein in a similar fashion to the estimation of energy band gaps in peptides and polypeptides [27].

9. THERMAL STABILITY: DESIGN OF THERMALLY STABLE MUTANTS OF bR

Thermal robustness is a mandatory requirement for any photoexcitable molecule to be used in BSSC. Our initial focus for many years has been on the thermal stabilization of bR without stripping it of its unique photochemistry by stabilizing the photointermediates and enhancing their life times in applications of bR in solar devices. Nanoelectronic devices based on bR require thermally robust mutants of bR. Therefore, increasing the thermostability of bR has been an area of intense research in our laboratories. One method of choice has been rational site-directed mutagenesis of bR. Advancements in thermostable vectors, antibiotic resistance genes, and the genetic characterization of extreme thermophiles have prompted the development of in vivo thermoselection systems to optimize mesophilic proteins bR for device applications *Thermus thermophilus* has been a useful in vivo screening platform for bR mutants for which a versatile, heat-stable expression vector is required. Mutants that retain structural stability at increased temperatures have been used as starting points for additional rounds of mutagenesis and thermoselection. Several iterations of thermoselection may be required before a bR variant with adequate thermostability can be used for device applications. In a recent study to optimize the heat capacity of bR, eight residues were selected in our studies. Mutations induced to confer thermal stability in bR were D85, W86, L93, D96, D115, W182, W189, and D212. Several of the bR mutants are stable in excess of 140°C.

9.1. Design of bR Mutants that would Facilitate Charge Separation and Increase Photovoltaic Efficiency

De novo site-directed mutations in bR to facilitate charge separation to design new mutants of bR expressly for the BSSC project are underway in our laboratories.

10. CHOICE OF LIGHT-HARVESTING PROTEINS AND THEIR MUTANTS

The choice of light-harvesting proteins has to be based on the following criteria:

1. Thermal stability
2. Maximal charge separation on photon absorption
3. Broadband absorption necessary to capture solar light
4. Simplicity of the electrolyte. It will be ideal to use a conducting polymer.
5. Environmentally friendly green sensitizers, wide gap semiconductors, and electrolytes thatare noncorrosive

The structure of the triple mutant of bR, [E9Q/E194Q/E204Q] bR (Figure 4) where three Glu residues at positions 9, 194, and 204 are mutated to attenuate the protonation pathway could potentially be useful in solar cell design.

11. PHOTOSYSTEMS I AND II

Photosystems are made of several protein subunits, as well as hundreds of cofactors, and act as large complex. The photosytems are contained within the chloroplasts in the leaves of plants.

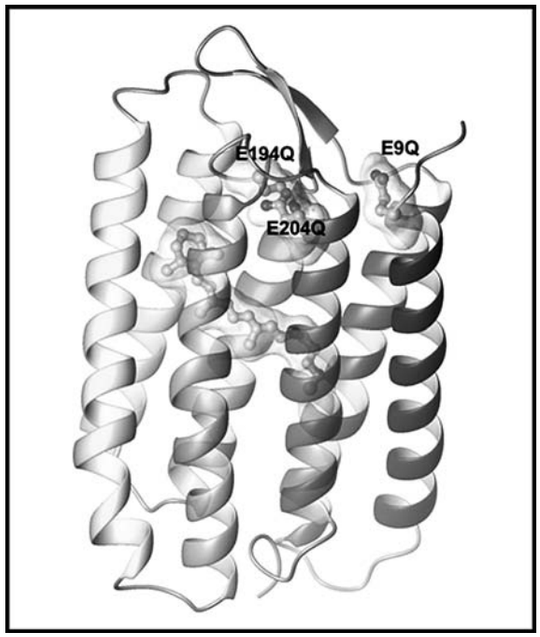

Figure 4. Structure of [E9Q/E194Q/E204Q] bR.

Two types of photosystems exist: photosystem I (P700) and photosystem II (P680). Each photosystem is differentiated by the wavelength of light to which it is most reactive (700 and 680 nanometers, respectively), and the type of terminal electron acceptor. Type I photosystems use ferredoxin-like iron-sulfur cluster proteins as terminal electron acceptors, whereas type II photosystems ultimately shuffle electrons to a quinone terminal electron acceptor.

A photosystem is made up of a reaction center pigment of chlorophyll *a* and numerous antenna pigments and proteins (Figure 5). Because chlorophyll *a* can only absorb light of a narrow wavelength, it works with the antenna pigments to gain energy from a larger part of the spectrum. The pigments absorb light of various wavelengths and pass along their gained energy to the reaction center chlorophyll. When the energy reaches the chlorophyll *a*, it releases two

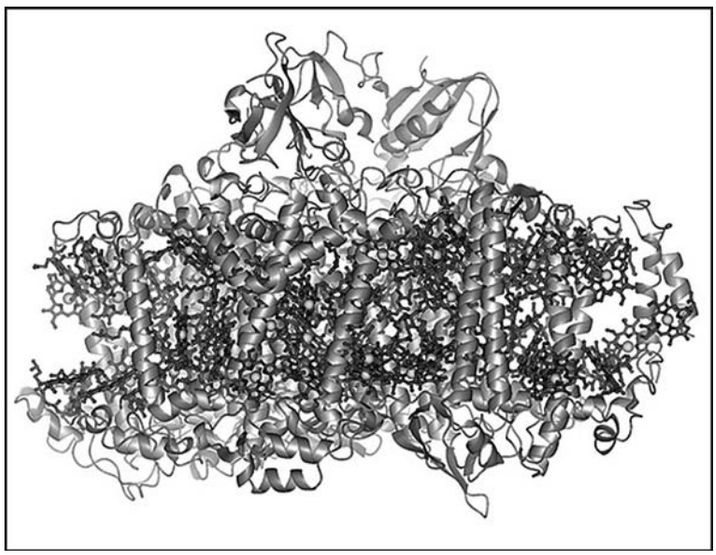

Figure 5. Photosystem I from Protein Data Bank Code: 1jb0.

electrons into an electron transport chain. Chlorophyll *a* normally has an optimal absorption wavelength of 660 nanometers; it associates with different proteins in each type of photosystem to slightly shift its optimal wavelength, producing two distinct photosystem types. Other proteins serve to support the structure and electron pathways in the photosystem.

When photosystem II absorbs light, electrons in the reaction-center chlorophyll are excited to a greater energy level and are trapped by the primary electron acceptors. To replenish the deficit of electrons, electrons are extracted from water (either through photolysis or enzymatic means) and supplied to the chlorophyll. Photoexcited electrons travel to photosystem I through an electron transport chain set in the thylakoid membrane. This energy decrease is harnessed (the whole process is termed chemiosmosis), to transport H^+ ions through the membrane to provide a proton-motive force to generate ATP. If electrons only pass through once, the process is termed noncyclic photophosphorylation. When the electron reaches photosystem I, it fills the electron deficit of the reaction-center chlorophyll of photosystem I. The deficit is caused by photo-excitation of electrons, which are again trapped in an electron acceptor molecule, this time that of photosystem I. These electrons may either go through the aforementioned electron transport chain again, in which case it is termed cyclic photophosphorylation. Otherwise, the electrons pass down another electron transport chain, which ends at an enzyme, NADP+ reductase. Electrons and hydrogen ions are added to NADP+ to form NADPH. This reducing agent is transported to the Calvin cycle to react with glycerate 3-phosphate, along with ATP to form glyceraldehyde 3-phosphate, the basic building block from which plants can make a variety of substances.

Scientists have long observed that photosynthesis is a highly efficient process of harvesting sunlight and converting it to chemical energy [28]. Each photon absorbed by the photosynthetic mechanism has a nearly 100% probability of conversion into an energetic electronic state that powers the plant's carbon-fixing and water-splitting reactions. In 1991, this process inspired researchers to design "excitonic" solar cells (as opposed to the p-n junction Si-based) called DSSCs that have recently reached a 11.3% laboratory efficiency, achieved by using mesoporous TiO_2 nanostructures as the substrate for the light-absorbing pigment to increase the surface area exposed to sunlight. DSSCs are still expensive to manufacture and have limited lifetimes. In addition, they have only increased from 7.5 to 11.3% in efficiency in more than 15 years of active research. The scientists behind DSSCs could not use the photosynthetic proteins directly because no way of keeping them functional in artificial environments existed. Nowadays, designed, synthetic surfactant peptides, discovered by Shuguang Zhang, have allowed us to keep membrane proteins, including PS-I active and "alive" for extended periods of time.

Das et al. at MIT have shown that it is possible to immobilize and keep "alive" the proteins at the center of photosynthesis (photosystem-I and reaction centers) on artificial, dry, flat chips connected to microelectronic circuits that are in turn powered by sunlight converted to electricity by these proteins [17]. This was a first step, a demonstration of principle of what is possible. There is no reason, in principle, why we cannot learn how to use plant matter extracts to create photosynthetic electric "paint" that can be spread on conducting surfaces and covered with a transparent, conducting, protective layer (the second electrode) to generate useful electricity. With a paint approach, what matters most in a viable solar power application is not the efficiency but the final cost per kilowatt hour as there are large areas available for painting and the raw materials are cheap. It is of course possible to increase the efficiency of such paint by spreading it over suitable, high-surface area nanostructures such as ZnO nanowires, which our laboratory has started doing.

Photosynthetic electric power has the attractive advantage of being potentially extremely low cost: plants use the sun to make proteins that we can use to harvest solar power for human needs. If the process of extracting, purifying, drying, and keeping functional is made using little energy, we have a long-term solution that can only get better with time as we "domesticate" the molecules to be sturdier and more efficient.

To investigate how one goes about harvesting sunlight using the proteins at the core of photosynthesis, our group has already purified Photosystem I from a variety of plants and bacteria, modified it to be suitable for oriented attachment to ZnO-nanowire surfaces, and we are currently trying to elucidate the I-V characteristics of these devices. Our progress so far shows us the next incremental steps we must take:

1. Increase the lifetime of the proteins (currently at 3 weeks) by matching them to tailor-made protective surfactant peptides
2. Characterize binding affinities of various binding motifs: "domestication"
3. Match hole-transport layers to increase efficiency and stability and power rate devices

4. Based on knowledge from steps 1, 2, 3, develop "paint" processes
5. Characterize and test performance of "paint"
6. Further "domesticate" the molecules using knowledge gained from steps 4 and 5
7. Steps 1-6 must be achieved while always striving to minimize the (energy) cost of each processing step

After demonstrating the proof of principle [17, 29], the first step toward photosynthetic, photovoltaic paint is the extraction of sufficient amounts of Photosystem I from appropriately chosen plants.

Such paint can be applied to a variety of conducting flexible polymers in a roll-to-roll process or applied to immobile conducting surfaces such as roofs. Although our initial experiments where done with spinach Photosystem I and bacterial reaction centers, we have concentrated our purification efforts on plants that are likely to be easy to use in the future if and when massive amounts of Photosystem I are needed. These are trees (used by the logging and paper industries that pay companies to dispose of the green leaves of cut trees) such as maple, oak, and pine. We have also purified Photosystem I from bamboo and seaweed. We chose to add seaweed for two reasons. Firstly, we suspect that because seaweed thrives in a light-starved environment, it may have developed a Photosystem I of greater efficiency. During this project, we will be able to characterize the efficiency of seaweed Photosystem I as compared with other plants. Second, the "invasion" of aggressive seaweed species in north Mediterranean coasts as well as Southern California more recently suggests that cleaning up the seabed from such seaweed would be significantly easier if there was a use and thus a value to it as raw material for photosynthetic, photovoltaic paint [30].

11.1. Step 1: Increasing the Lifetime of Photosystem I in Dry State

Our preliminary work has shown it is possible to match synthetic, designed surfactant peptides to stabilize Photosystem I [16]. By further iteration and a large-scale assay of various peptides and cocktail of peptides, we are confident we can extend the stability of the PS-I complex to well beyond the 3-week period achieved.

11.2. Step 2: Characterize Binding Affinities of Various Binding Motifs: "Domestication"

Binding the Photosystem I molecule in a particular orientation is very important to our application (as random orientation would give zero net current). To ensure strong, nondenaturing and oriented binding of Photosystem I to the electrode surface, we have developed the technique of subunit exchange. In brief, we insert a known ZnO binding amino acid sequence into one of the Photosystem I subunits near the side we wish to make "sticky" (the psa-D and psa-E subunits). We call the modified molecules "domesticated" because they now behave in a way useful to humans as opposed to their "wild" counterparts.

11.3. Step 3: Match Hole-Transport Layers to Increase Efficiency and Stability and Power Rate Devices

Several charge transport layers such as organic semiconductors (e.g, Alq3, C60) as well as PEDOT and other polymers will be tested for efficient coverage and biocompatibility while building dry, flat, and ZnO-based devices. Standard 0.5-cm $\times$ 0.5-cm devices will be tested under solar simulated illumination and sent to the National Renewable Energy Laboratory (NREL) for official power ratings. Larger devices, 10 cm $\times$ 10 cm, will be constructed and tested to check scalability.

11.4. Step 4: Based on Knowledge from Steps 1, 2, and 3, Develop "Paint" Processes

Steps 1, 2, 3 are based on a high-surface area ZnO substrate. We will adapt the Photosystem I by adding different binding motifs to different surfaces, such as conducting flexible polymers or conducting oxide films so that it can be attached proper side up on any shape surface. We will chose the best charge transport layer material found in Step 2 to spray paint on top of the Photosystem I and test the scalability, electrode placement and lifetime of the photosynthetic, photovoltaic paint.

11.5. Step 5: Characterize Lifetime and Performance of Photovoltaic Paint

By IV testing, similar to that in steps 1 and 3, and by using identical setups, we will characterize the lifetimes and performance of photovoltaic paint. We will send a sample to the NREL for

official, independent power rating under solar illumination as is the standard for the better solar labs around the world.

11.6. Step 6: Further "Domesticate" the Molecules Using Knowledge Gained from Steps 4 and 5

After paint characterization, we can iterate "domestication" and charge transport layer choice steps to optimize performance and lifetime.

11.7. Step 7: Steps 1-6 Must Be Achieved While Always Striving to Minimize the (Energy) Cost of Each Processing Step

Because our goal is to develop a realistic, nonsilicon-based solar power conversion technology that is easy to apply and cost-efficient, in every step, of our research, we will be concerned with the cost, both direct (raw materials, energy spent) and indirect (amount of expertise and high technology needed), and will try to invent processes that are low-tech, low-temperature, and low cost so that we do not end up in the all-too-frequent situation where a technology works in the laboratory but is too costly to scale up and commercialize.

12. POTENTIAL ELECTRODE CANDIDATES

This section gives a detailed account of two electrode materials based on TiO_2 nanofibers and ZnO nanowires.

12.1. TiO_2 Nanofibers

12.1.1. Fabrication of TiO_2 Nanofibers

Nanostructured metal oxide ceramics, for example, TiO_2 and ZnO, have received a greater attention because of their novel opto-electrical properties and their applications in being a photocatalyst and as a wide band-gap semiconducting electrode for DSSCs. Conventional DSSCs use a layer of TiO_2 nanoparticles because of high surface area for dye attachment. But, in case of the nanoparticle layer, the greater surface states act as recombination centers and the efficiency is limited by the inefficient transport of electron-hole pair. The one-dimensional metal-oxide electrode, such as a nanowire and nanofiber, serves this purpose of efficient collection and transport of electron-hole from the point of photo-generation to the conductive substrate. In case of DSSE incorporating nanowires, the reported energy conversion efficiency has not been high. The maximum conversion efficiency reported in case of ZnO nanowires are approximately 1.2 to 1.5% [31]. This not-so-high efficiency in nanowires is because of lower aspect ratio and lower surface area for the dye attachment. The nanofiber surpasses nanowires in this regard because of its greater aspect ratio, high surface area, and uncomplicated, cost-effective manufacturing technique. High conversion efficiencies reported with electrospun TiO_2 supports the concept and indicates promising scope [32].

Spray deposition (Figure 6) offers a simple and cost-effective technique for the fabrication of polymer and ceramic nanofibers [33]. In a typical spray deposition technique to fabricate ceramic fibers, the precursor in mixed in a particular proportion with the polymer solution and is extruded by applying high voltage. The metal oxide-polymer composite nanofiber is then annealed at high temperature to get ceramic fibers. The high temperature annealing serves two purpose; first, it removes the polymer and, second, it also simultaneously helps in the crystallization of the metal oxide ceramic.

The average diameter of the fibers can be tailored from micron to tens of nanometer by tuning the spinning and the annealing conditions (Figure 7). Also, a broad range of ceramic systems and composite ceramic systems can be manufactured by electrospinning. Moreover, by suitable spinning techniques, aligned and stacked nanofiber electrodes can also be fabricated. This organized electrode mesh can enhance the collection and transportation of electron-hole pair [34].

12.1.2. Nanofibrous Architecture for DSSC

Several groups are working on replacement the TiO_2 nanoparticles layer with nanofiber or with hybrid architecture of the nanoparticles and nanofibers. Katsuhiro et al. [35] have achieved an efficiency of more than 4% on TiO_2 nanofiber DSSC with 1 cm^2 working area. It was also

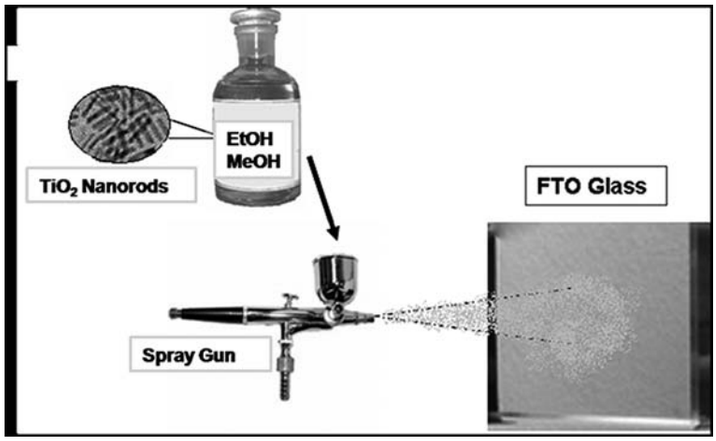

Figure 6. A schematic showing spray deposition of TiO_2 nanorods on the surface of FTO glasses. Reprinted with permission from [33], K. Fujihara et al., *Nanotechnology* 18, 365709 (2007). © 2007, IOP Publishing.

reported in the literature by Mu et al. [32] an overall conversion efficiency of 6.2% by using electrospun TiO_2 nanofibers composed of 1-D aligned fibrils with a 0.16-cm^2 working area. They also studied the phase separation between the precursor and polymer matrix during electrospinning and used the concept to make nanofibrils for DSSE electrode. The peeling off of the ceramic membrane from the conductive substrate has proved a limiting factor for increasing efficiency but, as recently reported, with the solvent treatment [32, 35] and pressure application the limitation can be overcome and the higher efficiency can be achieved. In our laboratory, the nanofiber layer of several microns has been achieved with proper adhesion on ITO/FTO substrate.

Another direction of research work for DSSC in which nanofiber architecture has proved superior is the use of the solid electrolyte. Leaking and evaporation of liquid electrolyte has been a serious problem in DSSCs. The use of solid electrolyte serves a viable solution but, because of inefficient contact between the solid electrolyte and TiO_2 nanoparticles, the conversion efficiency has been very low [36, 37]. Nanofibers with its higher interfiber porous structure than TiO_2 nanoparticles layer (nanofibers $>$500 nm, nanoparticles $\simeq$50–100 nm) enhances the penetration of solid electrolyte inside electrode layer and can enhance the efficiency [32].

12.1.3. Proposed Nanofiber-Nanoparticles Architecture

Because the nanofibers has been proved for superior transport and the nanoparticles has been proved for more dye attachment, a multilayer structure or hybrid structure electrode has been proposed for greater light harvesting and less recombination losses. This multilayer electrode

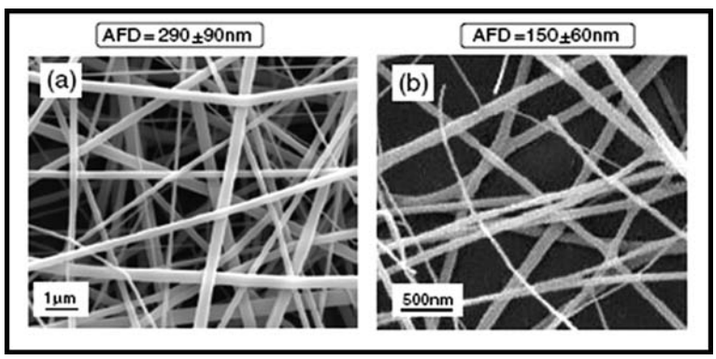

Figure 7. SEM images of (a) as spun metal-oxide composite fibers and (b) TiO_2 ceramic fibers. Reprinted with permission from [33], K. Fujihara et al., *Nanotechnology* 18, 365709 (2007). © 2007, IOP Publishing.

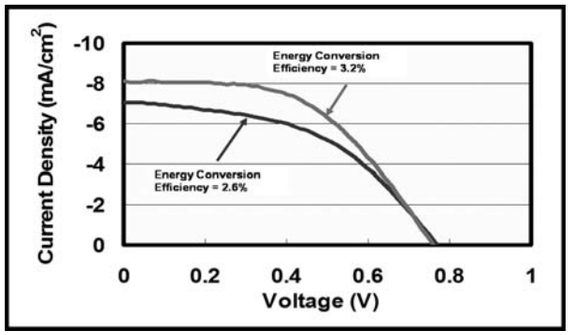

Figure 8. I-V graph of TiO_2 nanofiber DSSC.

layer consists of a nanofiber layer sandwiched between the small nanoparticles layer and large nanoparticles layer. With this multilayer architecture a photocurrent density of 8 mA/cm^2 and energy conversion efficiency of 3.2% had been achieved in our lab (see, Figure 8).

12.2. Zinc Oxide Nanowires

Semiconducting II-VI zinc oxide (ZnO) is a potential candidate for different applications in next generation of optoelectronics devices. The electrical, optoelectronic, and photochemical characteristics of ZnO has made it one of the most widely used materials among other metal oxides. Zinc oxide nanoparticles, nanowires, and nanobelts have been demonstrated to be interesting material for a variety of applications [38]. However, it has been reported that nanostructured zinc oxide materials are very difficult to control as well as having a high temperature synthesis [39].

In case of gas phase synthesis (i.e., chemical vapor deposition, metalorganic chemical vapor deposition, pyrolysis, etc.), the molecular precursor is allowed to react at high temperature in the gas phase or as molecular solids. Not only that, during the reaction, nucleation, growth, and coalescence process take place simultaneously, generally leading to high possibility of structural disorder and without defined shapes, making the extraction of structural information on nanocrystal surfaces very difficult. However, in sol-gel technique, a solvent is used as the reaction medium and normally the process temperature is relatively very low.

There are many other advantages in using wet chemistry for the synthesis nanomaterials. For example (1) proper mixing is possible at the molecular level of precursors; (2) reaction kinetics can be controlled by choosing the right solvent; (3) reaction, nucleation, and growth can be easily monitored and influenced; (4) controlled growth is possible by using appropriate ligands; (5) the mobility of the growth phase and growth termination by surface restructuring and capping is easier to handle; (6) further processes are easy to continue, such as film preparation, processable powder etc; and (7) ordered nanostructured materials can be synthesized as required.

A crucial part of the design of solar cells is the method of contacting them. Not only can shading and resistance losses have a significant impact on efficiency, but the contacting method also is often critically interwoven with other aspects of cell design, such as surface and contact passivation and front and rear reflectance. In addition, it is necessary to connect cells within thin-film modules in series and, for low-quality c-Si cells, there are potential advantages to be had from connecting like-polarity layers in parallel, thus enabling high carrier-collection-efficiencies [40, 41]. Of course, any contacting scheme should also be compatible with low-cost manufacturing processes. In this project, we will use ink-jet printing and screen printing methods to avoid high-cost vacuum based techniques for metal interconnections.

ZnO nanowires and structures that combine nanowires and nanoparticles were used as the wide band gap semiconducting photoelectrode in dye-sensitized solar cells. The nanowires provide a direct path from the point of photogeneration to the conducting substrate and offer alternative semiconductor network morphologies to those possible with sintered nanoparticles. Growing nanowires with dendrite-like branched structure greatly enhances their surface area, leading to improved light harvesting and overall efficiencies. Hybrid cells based on a combination of nanowires and nanoparticles can be tailored to take advantage of both the high surface area provided by the nanoparticles and the improved electron transport along a nanowire network. Solar cells made from branched nanowires showed photocurrents of 1.6 mA/cm^2, internal quantum efficiencies of 70%, and overall efficiencies of 0.5%. Solar cells made from appropriate

hybrid morphologies show photocurrents of 3 mA/cm^2 and overall efficiencies of 1.1%, while both the nanowire and hybrid cells show larger open-circuit voltages than nanoparticle cells.

Recently, we reported a study on the growth of highly anisotropic (aspect ratio >150) with almost no detectable increase in diameter (with time of hydrothermal growth) of zinc oxide nanowires at low temperatures on nonepitaxial substrates [42]. Results indicate that hexamine acts as a shape inducing surfactant by selectively capping the nonpolar crystallographic planes of the zincite crystal. We observe nanowires with typical diameters of ~30 nm and lengths exceeding several microns after a 24-h growth period at 60–95°C.

A wide range of strategies have been explored by different groups for the synthesis of nanowires of ZnO [1, 43, 44]. The conventional synthetic techniques for ZnO nanowires usually involve a high temperature, vapor-phase synthesis. It is a catalyst-driven synthesis that relies on the dissolution of the vapor of the semiconductor material like ZnO into metal nanoparticles (usually gold), followed by super-saturation and crystallization [45]. Various modifications of the high temperature vapor-solid method have been reported for the growth of ZnO nanostructures, including nanobelts and nanowires. The commercial potential for these processes are constrained by the need for an insulating and/or expensive substrate for proper-oriented growth of the nano-rods, and also the complexities and cost of the high temperature and controlled atmospheric systems. The need for deposition of a monolayer of gold nanoparticles on the substrate, to catalyze the epitaxial growth, further increases the complexity of the process.

Alternative low-temperature techniques for synthesis of nanowires of metal oxides usually involve a hydrothermal growth process inducing an epitaxial, anisotropic crystal growth in a solution [46, 47]. The hydrothermal process is usually substrate independent and offers a fairly good control over the morphology of the obtained nanowires [48]. Among the various synthetic techniques for obtaining nanowires of ZnO, the sol-gel based strategy involving hydrothermal growth of ZnO particles is probably the most energy efficient, by avoiding the complexities of vacuum environment and the need for high temperatures.

First reported by Vayssieres [49], this process involves epitaxial growth of ZnO rods on various substrates from an equimolar aqueous solution of zinc nitrate and hexamine as precursor. The technique relies on the inherent anisotropy in the crystal structure of ZnO (hexagonal Wurtzite) [50]. Because ZnO exhibits partial polar characteristics, an electric dipole is set up between the opposite ends of (001) plane of the zincite crystal, which leads to a high surface energy for the polar plane. Lower energy non-polar planes are more stable, thus in a thermodynamically stable growth process, large facets are usually the nonpolar planes [51].

Lowering the thermodynamic barrier by providing nucleation sites, which is achieved by fixing presynthesized ZnO nanoparticles on the substrate (seeding), improves the aspect ratio of the obtained rods and, according to recent reports [52], results in better uniformity. Nucleation sites can be introduced by depositing a layer of ZnO particles, spin coating a layer of colloidal ZnO nanoparticles obtained by chemical route.

Because the growth of nano-rods or wires (Figure 9) occur epitaxially from the seeds, a predetermined pattern of nanowires on the substrate can be achieved by patterning the deposition of the ZnO seeds, similar to reports of patterned growth of ZnO rods through the vapor phase route [53]. However, unlike the vapor phase route, the seeded hydrothermal growth can be achieved on a wide variety of substrates and at much lower temperatures.

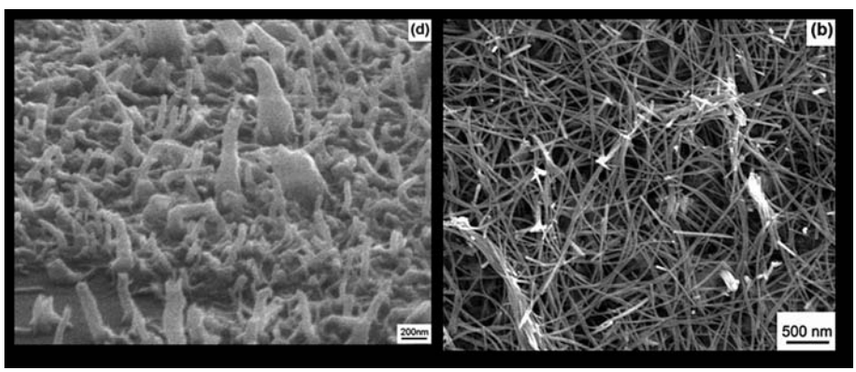

Figure 9. Left, SEM at a tilt of 65° showing the growth of the nanowires from the silicon substrate grown for 7 h in a chemical bath at 95°C; Right, SEM of ZnO nanowires grown for 24 h in a chemical bath at 95°C on a soda-lime glass substrate.

13. TRANSPARENT CONDUCTING OXIDE FILMS

Transparent oxide thin films tested for solar cells range from tin dioxide, indium tin dioxide, cadmium oxide, and zinc oxide, among others. Metal oxide coatings are generally conducting because of their inherent nonstoichiometry. However, the transparent conducting oxides (TCOs) are always doped to increase the carrier concentration to render the coating appropriately conducting to be suitable as an electrode. The TCO thin films are deposited by a variety of methods including chemical vapor deposition, spray pyrolysis, sputtering, evaporation, pyrosol, etc [54]. Atmospheric CVD techniques have been widely used for the deposition of metal oxide semiconductor materials. Sol-gel techniques have also been used for many years for successfully growing metal oxide transparent-conducting thin films for optoelectronic devices. Sol-gel techniques are quite suitable for industrial applications of metal oxide thin films and offer a unique possibility to be a competitive technique to the much-used sputtering processes. However, some optimizations still are required for specific processes related to sol-gel to be able to apply them to large-scale applications. Indeed, a comparison of the capabilities of these two processes will allow a fair view of the possibilities of applying either of the techniques for specific niche applications.

CVD, in retrospect, is a widely recognized process which, when conducted in the atmospheric pressure, does not need thorough equipments that are expensive and difficult to run. One such example of a simple CVD process is the pyrosol deposition process, which has even been demonstrated for industrial application for the coating of meter long glass substrates [55]. The pyrosol process is quite simple and leads to good-quality films. We can also propose a sol-gel-pyrosol process technique that will be interesting as colloids can be used to seed growth to give rise to controlled crystallite sizes and morphology of film materials. Such a process would be a natural evolution of the sol-gel and pyrosol techniques to be developed during the course of this project. We have already reported large area deposition of tin dioxide thin films on glass substrates using a novel pyrosol deposition technique for making flexible thin film transparent conducting oxide substrates [55–57].

13.1. Mechanism of Electronic Charge Shift in bR

Although bR can be used per se as an energy transducer or for the generation of H^+ ions, here we are combining its potential as a photoelectric with wide-gap semiconductors to exploit the salient features of both in the construction of a smart bio solar cell.

Upon absorption of light, there is a shift of electron density from the β-ionone ring of the chromophore toward the Schiff base, Figure 10. This shift is comparable with a 2.6-Å displacement of a single electron down the polyene chain [58] and is in the opposite direction of the initial photovoltage spike that is observed in bR [59].

This charge shift is so short in duration that no experimental method has yet been able to observe the voltage associated with the excitation process. However, this charge shift is a critical

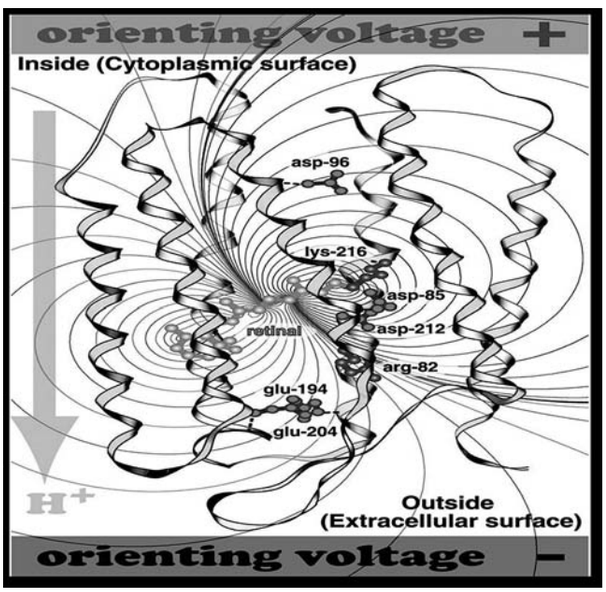

Figure 10. Shift of electron density from the β-ionone ring of the Chromophore towards Schiff base.

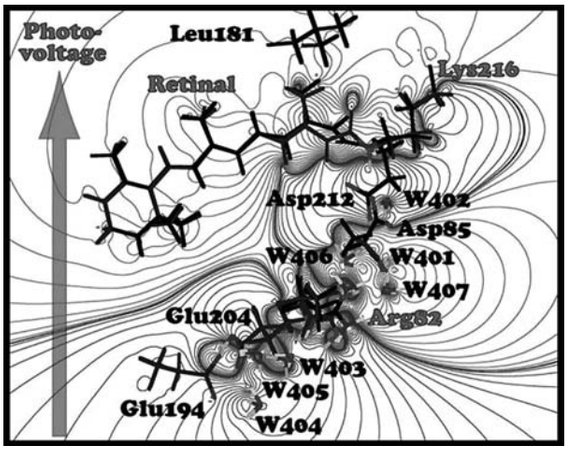

Figure 11. Charge shift make the imine linkage more negative and establishes repulsive interaction between this region of the Chromophore and the two nearby Asp residues 85 and 212.

component of the primary event because it sets in motion events that lead to the photoisomerization of the chromophore [60].

In particular, the charge shift makes the imine linkage more negative and establishes a repulsive interaction between this region of the chromophore and the two nearby aspartic acid residues (85 and 212; see Figure 11). This repulsion triggers a torsional photoisomerization about the 13-*cis* double bond of the chromophore [61–63]. It is generally believed that the initial photovoltaic signal (B1) reflects the photoisomerization of the chromophore during the primary event [64–66].

Electrostatics play a key role in charge separation and electron ejection. Electrostatic difference map associated with the formation of the K state has been reported recently by Fojan et al. [67]. The crystallographic data are from protein data bank entry 1M0P [68] bR differs from Chlorophyll family and PS-I and II. A schematic of the bR based bio solar cell is shown in Figure 12.

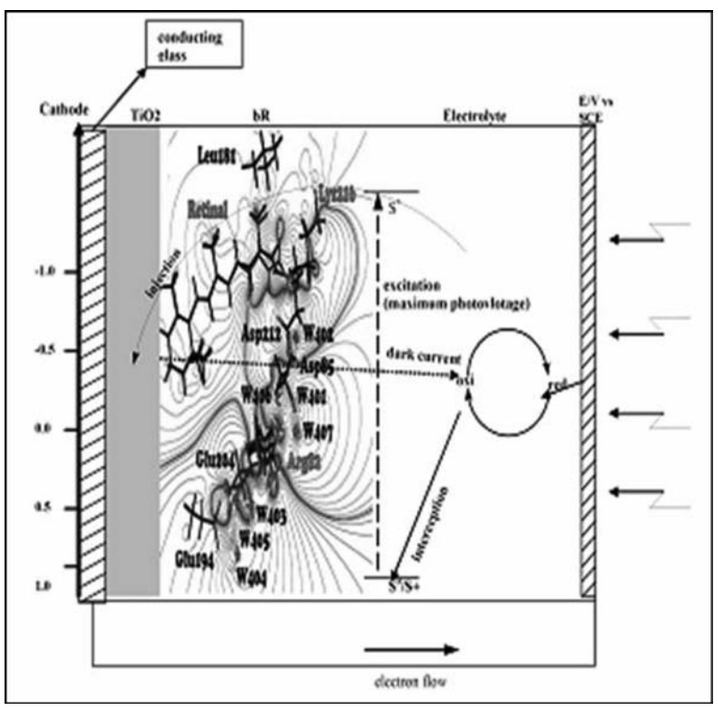

Figure 12. Schematic of bio solar cell.

Absorption of photons by bR is principally through the chromophoric group and the charge separation that occurs eventually leads to shedding of electrons whereas in the case of RuN_3, Ru^{3+}, chlorophylls, Mg^{2+}, and PSI, the iron-sulfur clusters play the key role. This is a major difference between bR and other sensitizers.

14. NANOMATERIALS AND FUEL CELLS

Proton exchange membrane fuel cells (PEMFCs) attract considerable interest as alternative power sources for low or zero emission vehicles as well as for stationary and portable applications due to their higher-power densities and environmental aptness [69, 70]. However, commercialization of PEMFC systems are constrained by factors such as, attaining maximum utilization of the platinum metal catalysts, and limited performance and durability associated with the membrane electrode assemblies [71]. Previous attempts to use carbon nanotubes as the platinum catalyst support did not succeed due to the lack of control of the particle size [72] to meet performance expectation of the PEMFC. Generally, the low catalyst activity [73] and mass transportation, mainly at the cathode, limit the power density values in PEMFCs. To date, efforts in improving the PEMFC performance have been focused through maximizing catalyst utilization by decreasing the catalyst nanoparticles on the carbon support, dispersing the platinum nanoparticles on the support uniformly and also by enhancing proton transport using a polymer electrolyte with the catalyst layer [74, 75].

With an objective to lower the cost, other electrocatalysts, such as metal porphyrins [76], metal oxides [77, 78], and ruthenium-based chalcogenides [79, 80], have been pursued by researchers over the years; however, their electrocatalytic activities are generally inferior to that of pure platinum. Therefore, a major breakthrough is desired to achieve superior performance and durability demanded for commercial viability of PEMFCs [81].

Gas diffusion layers (GDLs) are one of the major components of PEMFC that play a significant role on hydrogen/air system performance at high current density region [82]. Hence, it is important to have a GDLs with optimized pore size and gas transport characteristics to attain best performance of the fuel cell. The superior mechanical and electrical properties of carbon nanotubes [82–84] offer both mechanical robustness (to provide durability) and improved performance of the PEMFC by using them as catalysts support in the catalyst layer. More recently, Kongkanand et al. and Girishkumar et al. reported Pt and Pt-Ru alloy on single-walled CNT (SWCNT) synthesis and characterization toward PEMFCs and direct methanol fuel cell applications. However, earlier studies do not provide sufficient evidence of an improved performance in the actual PEMFCs fabricated using carbon nanotubes either due to the lack of control of the size of the catalyst over nanotube support or because of the meager distribution of the catalysts over the nanotube surface [85–90]. Very recently, we demonstrated a simple approach in which both proper distribution of the platinum catalyst over the CNT support and optimized catalyst nanoparticle size is obtained while ensuring the maximum utilization of the catalyst in a fuel cell at the same time. Because of their superior electrical properties, multi-walled carbon nanotubes (MWCNTs) serve as a good catalyst support material. Transmission electron microscopy images of the MWCNT-supported platinum electro-catalyst show uniform catalyst distribution with a particle size of about 6-8 nm (Figure 13a). In the process of using carbon nanotube components

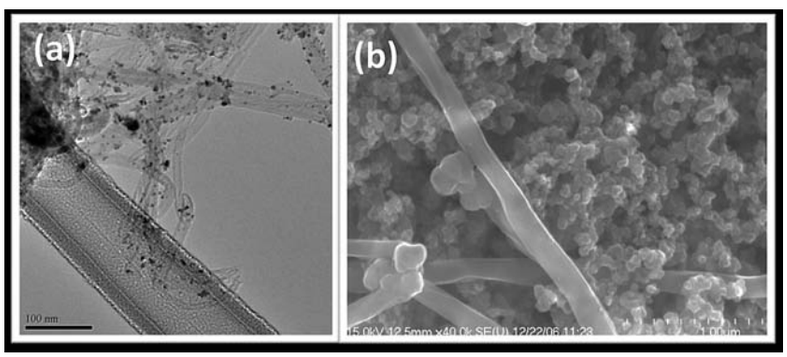

Figure 13. High-resolution TEM image of nanosized platinum on multiwalled carbon nanotubes and Scanning electron micrograph of surface of gas diffusion layer fabricated with graphitized carbon nanochain and nanofibers.

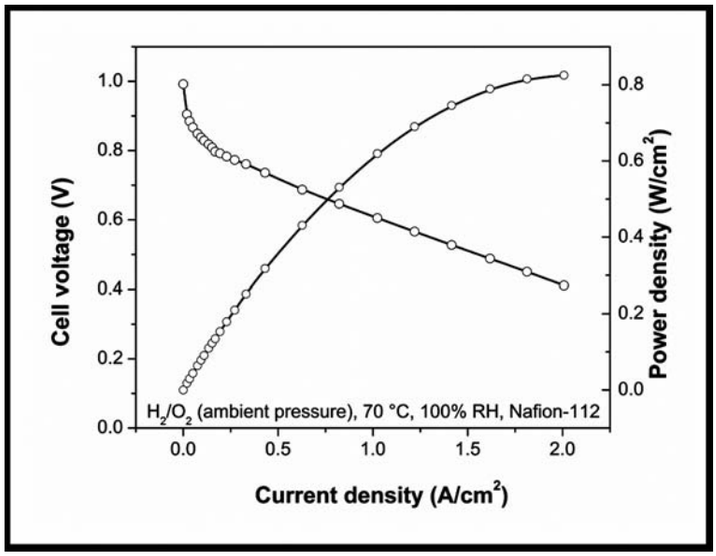

Figure 14. Galvanostatic polarization data for membrane electrode assembly at 70°C using Pt/MWCNT catalyst in two different dispersion agents, with PUREBLACK® 205–110 Carbon and single-walled carbon nanotubes (50/50 wt.%) based GDLs and Nafion-112 membrane as electrolyte with H_2/O_2 at ambient pressure.

for PEMFCs, we have also developed GDLs with different weight percentage combinations of PUREBLACK and SWCNTs. Scanning electron microscopy images of the GDL microstructure shows excellent surface morphology without any cracks on the micro-porous layer (Figure 13b). As seen in Figure 14, the membrane electrode assembly with SWCNT-based GDLs and MWCNTs supported Pt catalyst show power density as high as 0.8 W/cm^2 at 70°C using hydrogen/oxygen as reactants without any back pressure.

14.1. Biofuel Cells

Although biofuel cells (BFCs) have been known for almost one century, since the first microbial BFC was demonstrated in 1912 [91], the first enzyme-based BFC was reported only in 1964 using glucose oxidase (GOx) as the anodic catalyst and glucose as the biofuel [92]. The ability of a hydrogenase-coated electrode to catalyze efficient oxidation of hydrogen suggests exciting possibilities for use of such an electrode in a BFC, in which the conventional platinum fuel cell anode is replaced by a precious metal-free hydrogenase electrode. When the hydrogenase anode is coupled with a cathode incorporating the fungal enzyme (Figure 15), laccase, which catalyses

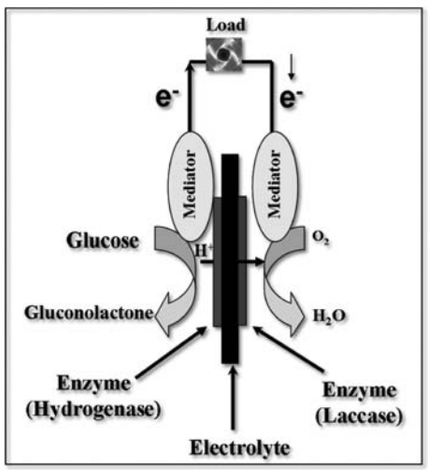

Figure 15. Operating principle of a biofuel cell involving hydrogenase and laccase enzymes.

reduction of oxygen to water, the hydrogenase biofuel cell produces a small-but-measurable power output. To improve the catalytic oxidation of bio-fuels, the GOx is attached to carbon nanotubes [93]. The ability of a hydrogenase-coated electrode to catalyze efficient oxidation of hydrogen suggests exciting possibilities for use of such an electrode in a BFC, in which the conventional platinum fuel cell anode is replaced by a precious metal-free hydrogenase electrode.

BFC generates electricity from carbohydrates (sugar), using enzymes as its catalyst through the application of power generation principles found in living organisms. The biobattery incorporates an anode consisting of sugar-digesting enzymes and mediator and a cathode comprising oxygen-reducing enzymes and mediator on either side of a cellophane separator. The anode extracts electrons and hydrogen ions from the sugar (glucose) through enzymatic oxidation as follows:

$$\text{Glucose} \rightarrow \text{Gluconolactone} + 2H^+ + 2e^-$$

The hydrogen ion migrates to the cathode through the separator. Once at the cathode, the hydrogen ions and electrons absorb oxygen from the air to produce water:

$$O_2 + 4H^+ + 4e^- \rightarrow 2H_2O$$

Through this process of electrochemical reaction, the electrons pass through the outer circuit to generate electricity (Figure 15). It is very interesting to note that the catalytic four-electron reduction of oxygen to water could take place at an enzyme electrode in a neutral solution. Because of the selective reaction at enzyme electrodes, the anode and cathode give no cross reaction to each other [94]. In general the BFCs could be classified into many types based on fuel containment, fuel, and catalysis sources; the origin of enzymes for biologically catalyzed devices; and the method of electron transfer between reaction site and electrode [95].

The major issues of BFCs that need to be resolved are lower power density and shorter enzyme stability. In particular, the promotion of the direct electron transfer (DET) reaction and the mutation of enzymes to tune the redox potential (to improve DET kinetics) are also very important challenges facing the commercialization of BFCs [96]. To address these two key issues, various enzyme immobilization methods have been attempted for constructing BFCs, such as adsorption, entrapment, and covalent attachment.

Recent advances in bionanotechnology are promising in their ability to improve the performance and stability of immobilized enzymes beyond the scope of these traditional approaches [97]. The large surface area provided by nanomaterials for the attachment of enzymes will increase the enzyme loading and possibly improve the power density of BFCs. Additionally, various nanostructured materials have shown great potential for stabilizing enzyme activity, which can be further used in improving the lifetime of BFCs. To promote DET of the protein and to improve the stability, it is necessary that the protein is immobilized in the form of clusters [93]. In this context, glucose oxidase (GOX) can be attached as crosslinked enzyme clusters (CECs) onto the surface of CNTs. In has been in a recent study that CEC-GOx showed no activity decrease for 250 days. The concept is depicted in Figure 16.

15. NANOMATERIALS AND HYDROGEN STORAGE

Nanostructured materials show potential in hydrogen storage because of their unique features, such as adsorption on the surface, inter- and intra-grain boundaries, and bulk absorption [98, 99]. Nanostructured and nanoscale materials strongly influence the thermodynamics and kinetics of hydrogen absorption and dissociation by increasing the diffusion rate as well as by decreasing the required diffusion length. In addition, the materials at the nanoscale offer the possibility of controlling

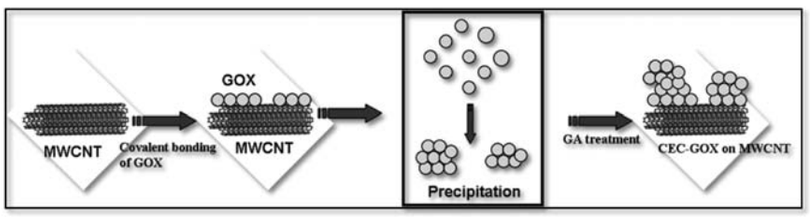

Figure 16. Schematic representation of reaction steps for covalently bonding GOX with MWCNTs.

material tailoring parameters independently than their bulk counterparts. They also lead to the design of light weight hydrogen storage systems with better hydrogen storage characteristics.

15.1. Carbonaceous Nanomaterials, CNTs, Fullerenes, and Nanofibers

Carbonaceous materials are attractive candidates for hydrogen storage because of a combination of adsorption ability, high specific surface, pore microstructure, and low mass density. Despite extensive results available on hydrogen uptake by carbonaceous materials, the actual mechanism of storage still remains a mystery. The interaction may either be based on van der Walls attractive forces (physisorption) or on the overlap of the highest occupied molecular orbital of carbon with occupied electronic wave function of the hydrogen electron, overcoming the activation energy barrier for hydrogen dissociation (chemisorption). The physisorption of hydrogen limits the hydrogen to carbon ratio to less than one hydrogen atom per two carbon atoms (i.e., 4.2 mass %). While in chemisorption, the ratio of two hydrogen atoms per one carbon atom is realized as in the case of polyethylene [100–102]. Physisorbed hydrogen has a binding energy normally of the order of 0.1 eV, whereas chemisorbed hydrogen has C–H covalent bonding, with a binding energy of more than 2–3 eV.

Dillon et al. presented the first report on hydrogen storage in carbon nanotubes and triggered a worldwide tide of research on carbonaceous materials [103]. Hydrogen can be physically adsorbed on activated carbon and be "packed" on the surface and inside the carbon structure more densely than if it has just been compressed. The best results achieved with carbon nanotubes to date confirmed by the NREL is hydrogen storage density corresponding to about 10% of the nanotube weight [104].

Fullerenes, on the other hand, is a new form of carbon with close-caged molecular structure, first reported by Smalley in 1985 [105]. It is a potential hydrogen storage material based on the ability to react with hydrogen via hydrogenation of carbon–carbon double bonds. The theory predicts that a maximum of 60 hydrogen atoms can be attached both the inside (endohedrally) and outside (exohedrally) of the fullerene spherical surface. Thus, a stable $C_{60}H_{60}$ isomer can be formed with the theoretical hydrogen content of ~7.7 wt.%. It seems that the fullerene hydride reaction is reversible at high temperatures. The 100% conversion of $C_{60}H_{60}$ indicates that 30 moles of H_2 gas will be released from each mole of fullerene hydride compound. However, this reaction is not possible because it requires high temperature approximately 823–873 K [106]. Solid C_{60} has face-centered cubic lattice at room temperature and its density is ~1.69 g/sm^3. Fullerene is an allotropic modification of carbon. Fullerene molecules are composed of pentagons and hexagons whose vertexes contain carbon atoms. Fullerene, C_{60} is the smallest and the most stable structure (owing to high degree of its symmetry).

Hydrogen can be stored in glass microspheres of approximately 50 μm diameter. The microspheres can be filled with hydrogen by heating them to increase the glass permeability to hydrogen. At room temperature, a pressure of approximately 25 MPa is achieved resulting in storage density of 14% mass fraction and 10 kg H_2/m^3 [107]. At 62 MPa, a bed of glass microspheres can store 20 kg H_2/m^3. The release of hydrogen occurs by reheating the spheres to again increase the permeability.

15.2. Nanocomposite Conducting Polymers

Nanocomposite material consisting of a polyaniline matrix, which can be functionalized by either catalytic doping or incorporation of nano variants are considered to be potential promise for hydrogen storage. It was reported that polyaniline could store as much as 6–8 wt% of hydrogen [108] which, however, another team of scientists could not reproduce [109]. Yet another recent study reveals that a hydrogen uptake of 1.4–1.7 wt% H_2 has been reported for the polymers of intrinsic microscopy [110]. Polyaniline is a conductive polymer, with conductivity on the order of 10^0 S/cm. This is higher than that of typical nonconducting polymers, but much lower than that of metals [111]. In addition to its conductivity, polyaniline emeraldine base is very simple and inexpensive to polymerize. It is because of this simplicity that it was chosen as a matrix material for the nanocomposite structure. Before such materials could be added, however, the performance of the polyaniline by itself had to be tested and compared to previous scientific data. Several different filler materials in various concentrations were added to the nanocomposite and its effect on the characteristics of the material determined.

Functionalization can be conducted by introduction of chemical groups into a polymer molecule or conversion of one chemical group to another group, which leads to a polymer with chemical, physical, or other functions. Functional polymer act as a catalyst, to bind selectively to

particular species, to capture and transport electric charge or energy, to convert light into charge carriers and vice versa.

15.3. High Surface Area Sorbents and New Materials Concepts for H_2 Storage

There is a pressing need for the discovery and development of new reversible materials. One new area that may be promising is that of high surface area hydrogen sorbents based on microporous metal–organic frameworks. Such materials are synthetic, crystalline, and microporous and are composed of metal/oxide groups linked together by organic struts. Hydrogen storage capacity at 78 K (–195°C) has been reported as high as 4 wt.% via an adsorptive mechanism, with a room temperature capacity of approximately 1 wt.% [112]. However, because of the highly porous nature of these materials, volumetric capacity may still be a significant issue.

Another class of materials for hydrogen storage may be clathrates [113], which are primarily hydrogen-bonded H_2O frameworks. Initial studies have indicated that significant amounts of hydrogen molecules can be incorporated into the sII clathrate. Such materials may be particularly viable for off-board storage of hydrogen without the need for high pressure or liquid hydrogen tanks.

16. NANOMATERIALS AND SOCIETY

Nanotechnology is viewed as a transformative technology that has the potential to stimulate scientific innovation while greatly benefiting society. However, the enthusiasm with which the scientific and technical communities are embracing the technology is being tempered by concerns over possible downsides, including risks to human health. The safety concerns of nanotechnology in energy conversion and storage would be thoroughly discussed. Nanotechnology is leading to the development of new materials and devices in many fields that demonstrate nanostructure-dependent properties. However, concern has been expressed that these same properties may present unique challenges when addressing potential health impact. Airborne particles associated with engineered nanomaterials are of particular concern, as they can readily enter the body through inhalation. Research into the potential occupational health risks associated with inhaling engineered nanostructured particles is just beginning [114, 115].

Maynard and Kuempel [115] explore this idea further, noting that the scale-dependent properties of nanomaterials are not necessarily associated with particle diameter but with material. Although these two criteria relate to inhalation exposure, they are sufficiently broad to encompass all potential routes of exposure, and provide a useful working framework for distinguishing between materials and products that are less likely to present health risks than those that are more likely to have some adverse health implications.

Major ecological concerns associated with sustainability of nanotechnological methods for the production and functional implementation of nanoparticles are thoroughly discussed in a review in the literature [116]. Nanotechnology could be highly beneficial in catalytic applications; however, their dispersion in the environment could make it impossible to take remediative action if safety issues pose concern [117]. Hopefully, governments and industry around the world will continue to ensure relevant risk-research is appropriately directed and well-funded, and that new research will mark a significant reduction in uncertainty over how to assess and manage the risk to health of engineered nanomaterials in the workplace [118].

17. NANOMATERIALS AND TOXICITY

An understanding of the behavior of airborne CNTs is critical for the development of CNT-based biosolar and fuel cells. Air-borne CNTs appear to move by convection and deposit in the respiratory tract by diffusion. SWCNTs, because of strong van der Waals forces, self-organize into ropelike structures that can range in lengths up to several microns. The potential hazards of inhaled CNT nanotubes have not been sufficiently evaluated, although the results of several in vitro and nonaerosol-associated in vivo studies suggest that exposure to these materials could represent a significant health and environmental hazard.

Respirable particles can be formed during nanotube growth, which are the main risk if inhaled [119]. It is therefore essential to investigate thoroughly the effects that CNT might have on human health and environment. CNT tend to form aggregates, many of which will not penetrate to the lung alveoli when inhaled. However, nonaggregated CNTs may, because of their small

size, penetrate to the alveoli of the lungs, where they may interact with surfactant proteins and lipids. Although in vivo toxicity studies previously reported represent an important first step in highlighting the possible risks associated with exposure to CNT, the protocols they rely upon may have produced artifacts that can be difficult to distinguish from effects produced by nanotubes themselves. Muller et al. [120] reported that, when multiwall CNT and ground CNT reach the lungs of mice, they are not eliminated and induce the formation of tumor necosis factor-α, a key mediator of inflammation, suggesting that CNTs are toxic. Increased cytokine expression, lung tumors, inflammation, and hyperplasia of epithelial cells have been observed during inhalation of nanoparticles [121–124]. Warhier et al. [125] reported airway obstruction in rats. An increase in cytotoxicity by 35% was observed when macrophages were incubated with SWNTs and MWNTs [126]. Fiber shape, length, and the aggregation of nanotubes can also induce immunological response in lungs [127].

Because of the resistance offered by high bond energy of carbon backbone, MWCNTs are nonbiodegradabele and are retained in the liver [128]. Multiple lesions in lung histology with abnormal lung resistance were reported by Huczko et al. [129] in animals exposed to CNT samples. Pharyngeal aspiration of SWCNTs led to granuloma formation, intestinal fibrosis, and alveolar thickening in mice [130], in addition to changes in pulmonary functions and decreased bacterial clearance [131]. The ecosystems may be affected through inadvertent or intentional releases of engineered nanomaterials. Nanoscale particles may affect aquatic or terrestrial organisms differently than larger particles because of their potential to cross and/or damage cell membranes and differences in other chemical and physical properties.

ACKNOWLEDGMENTS

S. Ramakrishna, V. Renugopalakrishnan, and T. Velmurugan would like to express thanks to the NUS President's office special program fund. V. Renugopalakrishnan also expresses his thanks to NSF, the Wallace H. Coulter Foundation, USAFOSR, ONR, NIH, and Harvard Medical School. Work in the EP laboratory has been supported by the Dirección General de investigación (MCYT) grant BFU2006-04656/BMC. A. M. Kannan would like to thank Arizona State University for financial support through ASU-ITESM (Mexico) Renewable Energy grant.

REFERENCES

1. Y. B. Li, *Appl. Phys. Lett.* 81, 144 (2002).
2. B. Yao, *Biosensors and Bioelectronics* 19, 283 (2003).
3. J. Xu, *Optical Materials* 22, 321 (2003).
4. P. Bertoncello, *IEEE Trans. Bionanoscience* 2, 124 (2003).
5. H. G. Choi, *Synthetic Metals* 117, 141 (2001).
6. R. Toth-Boconadi, *J. Photochem. Photobiol. B: Biol.* 65, 122 (2001).
7. C. Nicolini, *Biosensors & Bioelectronics* 14, 427 (1999).
8. L. Yuan, *Thin Solid Films* 340, 262 (1999).
9. M. Gratzel, *Inorg. Chem.* 44, 6841 (2005).
10. M. Gratzel, *Nature* 414, 338 (2001).
11. M. Gratzel, *MRS Bull.* 30, 23 (2005).
12. V. Renugopalakrishnan, S. Khizroev, H. Anand, P. Li, and L. Lindvold, *IEEE Trans. Magnetics* 43, 773 (2007).
13. W. Wang, *Biosensors and Bioelectronics* 21, 1300 (2006).
14. A. G. Manoj, *Biosensors and Bioelectronics* 19, 1067 (2004).
15. L. Lensu, *Optic Mater.* 27, 57 (2004).
16. P. Z. Kiley, *Public Library of Science* 3, 1181 (2005).
17. R. Das, P. J. Kiley, M. Segal, J. Norville, A. A. Yu, L. Wang, S. A. Trammell, et al., *Nano Letters* 4, 1079 (2004).
18. J. Zhao, *Electrochim. Acta* 47, 2013 (2002).
19. M. T. Giardi, *Trends Biotechnol.* 23, 257 (2005).
20. Q. Li, *Biosensors and Bioelectronics* 19, 869 (2004).
21. Y. Lu, *Langmuir* 21, 4071 (2005).
22. A. Yutaka, *Biosensors and Bioelectronics* 19, 843 (2004).
23. A. Kay and M. Gratzel, *J. Phys. Chem.* 97, 6272 (1993).
24. A. Kay, R. H. Baker, and M. Gratzel, *J. Phys. Chem.* 98, 952 (1994).
25. Y. Lu, *Langmuir* 21, 4071 (2005).
26. C. Bauer, G. Boschloo, E. Mukhta, and A. Hagfeldt, *Int. J. Photoenergy* 4, 17 (2002).
27. V. Renugopalakrishnan, in "Bionanotechnology: Proteins to Nanodevices" (V. R. and R. V. Lewis, Eds.), pp. 117–139, Springer, Dordrecht, The Netherlands, 2006.

28. A. Ke, "Photosynthesis Photobiochemistry and Photobiophysics," Dordecht: Kluwer Academic Publishers, 2001.
29. P. Ball, *Nature* 429, 823 (2004).
30. T. Bailey, B. J. Smith, B. J. Choi, M. Colburn, M. Meissl, S. V. Sreenivasan, J. G. Ekerdt, and C. G. Willson, "Step and Flash Imprint Lithography: Defect Analysis," *J. Vac. Sci. Tech. B* 19(6), 2806 (2001).
31. L. Matt, *Nat. Mater.* 4, 455 (2005).
32. J. S. Mu, *J. Macromol. Sci. A.* 42, 1529 (2005).
33. K. Fujihara, A. Kumar, R. Jose, S. Ramakrishna, and S. Uchida, *Nanotechnology* 18, 365709 (2007).
34. Z. Marke'ta, *Nano Lett.* 5, 1789 (2005).
35. O. Katsuhiro, *Nanotechnology* 17, 1026 (2006).
36. K. Wataru, *J. Phys. Chem. B.* 107, 4374 (2003).
37. B. O. Regan, *Chem. Mater.* 14, 5023 (2002).
38. H. Cao, *Appl. Phys.* 82, 303 (2002).
39. H. Ihara, "Encyclopedia of Nanoscience and Nanotechnology," American Scientific Publishers, 10, 1 (2003).
40. J. M. Gee, Proc. 23rd IEEE PVSC, 265 (1993).
41. A. Edmiston, *Prog. Photovoltaics* 3, 333 (1995).
42. A. Sugunan, in "Proceedings of the NATO Advanced Study Institute on Nanostructured and Advanced Materials for Applications in Sensors, Optoelectronic and Photovoltaic Technology, NATO Science Series II: Mathematics, Physics and Chemistry," Vol. 204, Bulgaria, 2004.
43. L. Dong, *Appl. Phys. Lett.* 82, 1096 (2003).
44. H. Kim, *Appl. Phys. Lett.* 81, 2085 (2002).
45. M. Law, *Annu. Rev. Mater. Res.* 34, 83 (2004).
46. Y. Xia, *Adv. Mater.* 15, 353 (2003).
47. M. K. Hossain, *J. Metastable Nanocryst. Mater.* 23, 27 (2005).
48. L. E. Greene, *Angew. Chem. Int.* 42, 3031 (2003).
49. L. Vayssieres, *J. Phys. Chem. B*. 105, 3350 (2001).
50. L. Vayssieres, *Adv. Mater.* 15, 464 (2003).
51. X. Y. Kong, *Appl. Phys. Lett.* 84, 975 (2004).
52. S. C. Liou, *J. Cryst. Growth* 274, 438 (2005).
53. L. Dong, *Appl. Phys. Lett.* 82, 1096 (2003).
54. J. Dutta, *J. Mat. Sci.* 30, 53 (1995).
55. J. Dutta, *Thin Solid Films* 239, 150 (1994).
56. D. Sweatman. In "International Conference on Nanoscience and Nanotechnology," 3–7, July, Brisbane, Australia, 2006.
57. J. Dutta, in "Proceedings of the 6th European Conference on Applications of Surface & Interface Analysis (ECASIA 95)" (H. J. Mathieu, B. Reihl, and D. Briggs, Eds.), Wiley & Sons, Chichester and New York, 1996.
58. R. R. Birge, N. B. Gillespie, E. W. Izaguirre, A. Kusnetzow, A. F. Lawrence, D. Singh, Q. W. Song, E. Schmidt, J. A. Stuart, S. Seetharaman, and K. J. Wise, *J. Phys. Chem. B.* 103, 10746 (1999).
59. H. W. Trissl, *Biochim. Biophys. Acta.* 806, 124 (1985).
60. U. Zadok, A. Khatchatouriants, A. Lewis, M. Ottolenghi, and M. Sheves, *J. Am. Chem. Soc.* 124, 11844 (2002).
61. R. A. Mathies, C. H. Brito Cruz, W. T. Pollard, and C. V. Shank, *Science* 240, 777 (1988).
62. R. R. Birge, *Annu. Rev. Phys. Chem.* 41, 683 (1990).
63. L. Song, M. A. El-Sayed, and J. K. Lanyi, *Science* 261, 891 (1993).
64. G. Rayfield, "In Molecular and Biomolecular Electronics," (R. R. Birge, Ed.), pp. 561–575. American Chemical Society, New York, 1994.
65. G. I. Groma, J. Hebling, C. Ludwig, and J. Kuhl, *Biophys. J.* 69, 2060 (1995).
66. K. C. Hsu, G. W. Rayfield, and R. Needleman, *Biophys. J.* 70, 2358 (1996).
67. P. Fojan, T. Lazarova, C. Sanz, M. Kolinski, S. Filipek, M. Ortiz-Lombardia, C. S. Verma, L. Gurevich, S. B. Petersen, T. Velmurugan, S. Ramakrishna, V. Renugopalakrishnan, and E. Padros, *Biochemistry* (Communicated, Biochemistry, 2007).
68. B. Schobert, J. Cupp-Vickery, V. Hornak, S. O. Smith, and J. K. Lanyi, *J. Mol. Biol.* 321, 715 (2002).
69. R. Service, *Science* 296, 1222 (2002).
70. A. M. Kannan, V. Veedu, L. Munukutla, and M. N. Ghasemi-Nejhad, *Electrochemical and Solid State Lett.* 10, *B* 47 (2007).
71. H. A. Gasteiger, S. S. Kocha, B. Sompalli, and F. T. Wagner, *Appl. Catalysis B: Environmental* 56, 9 (2005).
72. C. Wang, M. Waje, X. Wang, J. M. Tang, R. C. Haddon, and Y. S. Yan, *Nano Lett.* 4, 345 (2004).
73. S. D. Thompson, L. R. Jordan, and M. Forsyth, *Electrochim. Acta* 46, 1657 (2001).
74. X. Sun, R. Li, D. Villers, J. P. Dodelet, and S. Désilets, *Chem. Phys. Lett*. 379, 99 (2003).
75. K. Yasuda and Y. Nishimura, *Mater. Chem. Physics* 82, 921 (2003).
76. H. Liu, L. Zhang, J. Zhang, D. Ghosh, J. Jung, B. W. Downing, and E. Whittemore, *J. Power Sources* 161, 743 (2006).
77. J. Prakash, D. A. Tryk, W. Aldred, and E. B. Yeager, *J. Appl. Electrochem.* 29, 1463 (1999).
78. L. Jörissen, *J. Power Sources* 155, 23 (2006).
79. L. Zhang, J. Zhang, D. P. Wilkinson, and H. Wang, *J. Power Sources* 156, 171 (2006).
80. S. S. Ozenler and F. Kadirgan, *J. Power Sources* 154, 364 (2006).
81. J. Zhang, K. Sasaki, E. Sutter, and R. R. Adzic, *Science* 315, 220 (2007).
82. A. M. Kannan and L. Munukutla, *J. Power Sources* 167, 330 (2007).

83. A. L. Dicks, *J. Power Sources* 156, 128 (2006).
84. M. S. Dresselhaus, G. Dresselhaus, and P. C. Eklund, In "Science of Fullerenes and Carbon Nanotubes," San Diego: Academic Press, 1996.
85. R. H. Baughman, A. A. Zakhidov, and W. A. de Heer, *Science* 297, 787 (2002).
86. M. Yu, O. Lourie, M. J. Dyer, K. Moloni, T. F. Kelly, and R. S. Ruoffet, *Science* 287, 637 (2000).
87. Y. Shao, G. Yin, Y. Gao, and P. Shi, *J. Electrochem. Soc.* 153, A1093 (2006).
88. A. Kongkanand, S. Kuwabata, G. Girishkumar, and P. V. Kamat, *Langmuir* 21, 2392 (2006).
89. G. Girishkumar, T. D. Hall, K. Vinodgopal, and P. V. Kamat, *J. Phys. Chem. B.* 110, 107 (2006).
90. A. Kongkanand, K. Vinodgopal, S. Kuwabata, and P. V. Kamat, *J. Phys. Chem. B.* 110, 16185 (2006).
91. M. C. Potter, *Proc. Royal Soc. B, Biol. Sci.* 84, 260 (1912).
92. T. Yahiro, S. M. Lee, and D. O. Kimble, *Biochim Biophys. Acta* 88, 375 (1964).
93. M. B. Fischback, J. K. Youn, X. Zhao, P. Wang, H. G. Park, H. N. Chang, J. Kim, and S. Ha, *Electroanalysis* 18, 2016 (2006).
94. I. Taniguchi, M. Kishikawa, M. Ohtani, D. Tabata, and M. Tominaga, "209th ECS Meeting," May 7–12, 2006, Denver, CO, Abstract no. 580.
95. R. A. Bullen, T. C. Arnot, J. B. Lakeman, and F. C. Walsh, *Biosens. Bioelectron.* 21, 2015 (2006).
96. Y. Kamitaka, S. Tsujimura, N. Setoyama, T. Kajino, and K. Kano, *Phys. Chem. Chem. Phys.* 9, 1793 (2007).
97. J. Kim, H. Jia, and P. Wang, *Biotechnol. Adv.* 24, 296 (2006).
98. E. G. Baburaj, F. H. Froes, V. Shutthanandam, and S. Thevuthasan, Interfacial Chemistry and Engineering, Annual report, 4–1 (2000).
99. R. Schulz, S. Boily, L. Zaluski, A. Zaluka, P. Tessier, and J. O. Strom-Olsen, *Innovation in Metallic Mater.* 529 (1995).
100. A. Zuttel, *Naturwissenschaften* 91, 157 (2004).
101. A. Viswanathan, M. Sankaran, and M. A. Schibioh, *Bull. Catalysis Soc. India 2*, 12 (2003).
102. M. G. Nijkamp, J. E. M. J. Raaymakers, A. J. Van Dillen, and K. P. De Jong, *Appl. Phys. A.* 72, 619 (2001).
103. A. C. Dillon, K. M. Jones, T. A. Bekkedahl, C. H. Kiang, D. S. Bethune, and M. J. Heben, *Nature* 386, 377 (1997).
104. P. M. F. J. Costa, K. S. Coleman, and M. L. J. Green, *Nanotechnology* 16, 512 (2005).
105. H. W. Kroto, J. R. Heath, S. C. O'Broem, R. F. Curl, and R. E. Smalley, *Nature* 318, 165 (1985).
106. V. Meregalli and M. Parrinello, *Appl. Phys. A.* 72, 143 (2001).
107. Y. Kojima, Y. Kawai, A. Koiwai, N. Suzuki, T. Haga, T. Hioki, and K. Tange, *J. Alloys Compounds* 395, 236 (2005).
108. Y. Y. Fan, A. Kaufmann, A. Mukasyan, and A. Varma, *Carbon* 44, 2160 (2006).
109. S. J. Cho, K. S. Song, J. W. Kim, T. H. Kim, and K. Choo, *Fuel Chem. Div. Prep.* 47, 790 (2002).
110. A. Panella, L. Kossykh, U. Dettlaff-Weglikowska, M. Hirscher, G. Zerbi, and S. Roth, *Synthetic Metals* 151, 208 (2005).
111. N. B. McKeown, B. Gahnem, K. J. Msayib, P. M. Budd, C. E. Tattershall, K. Mahmood, S. Tan, D. Book, H. W. Langmi, and A. Walton, *Angewandte Chemie Int. Ed.,* 45, 1804 (2006).
112. J. L. C. Rowsell, E. C. Spencer, J. Eckert, J. A. K. Howard, and O. M. Yaghi, *Science* 309, 1350 (2005).
113. F. Schuth, *Nature* 434, 712 (2005).
114. A. D. Maynard, *NanoToday* 1, 22 (2006).
115. A. D. Maynard and E. D. Kuempel, *J. Nanoparticle Res.* 7, 587 (2005).
116. V. Uskoković, *Technol. Soc.* 29, 43 (2007).
117. D. G. Rickerby and M. Morrison, *Sci. Technol. Adv. Mater.* 8, 19 (2007).
118. A. D. Maynard and David Y. H. Pui, *J. Nanoparticle Res.* 9, 1 (2007).
119. A. D. Maynard, P. A. Baron, M. Foley, A. A. Shvedova, E. R. Kisin, and V. Castranova, *J. Toxicol. Environ. Health* 67, 87 (2004).
120. J. Muller, F. Huaux, N. Moreau, P. Misson, J. F. Heilier, and M. Delos, *Toxicol. Appl. Pharmacol.* 207, 221 (2005).
121. C. Dasenbrock, L. Peters, O. Creutzenberg, and U. Heinrich, *Toxicol. Lett.* 88, 15 (1996).
122. K. E. Driscoll, J. M. Carter, B. W. Howard, D. G. Hassenbein, W. Pepelko, and R. B. *Baggs, Toxicol. Appl. Pharmacol.* 136, 372 (1996).
123. G. Oberdoster, J. Ferin, and B. E. Lehnert, *Environ. Health Perspect.* 102, 173 (1994).
124. K. J. Nikula, M. B. Snipes, E. B. Barr, W. C. Griffith, R. F. Henderson, and J. L. Mauderly, *Appl. Toxicol.* 25, 80 (1995).
125. D. B. Warheit, B. R. Laurence, K. L. Reed, D. H. Roach, G. A. M. Reynolds, and T. R. Webb, *Toxicol. Sci.* 77, 117 (2004).
126. G. Jia, H. Wang, L. Yan, X. Wang, R. Pei, and T. Yan, *Environ. Sci. Technol.* 39, 1378 (2005).
127. K. Donaldson, R. Aitken, L. Tran, V. Stone, R. Duffin, G. Forrest, and A. Alexander, *Toxicol. Sci.* 92, 5 (2006).
128. X. Deng, G. Jia, H. Wang, H. Sun, X. Wang, S. Yang, T. Wang, and Y. Liu, *Carbon* 45, 1419 (2007).
129. A. Huczko, H. Lange, M. Bystrzejewski, and Baranowski, Pulmonary toxicity of 1-D nanocarbon materials. *Fullerenes Nanotubes Carbon Nanostruct.* 13, 141 (2005).
130. A. A. Shvedova, E. R. Kisin, R. Mercer, A. R. Murray, V. J. Johnson, and A. I. Potapovich, *Am. J. Physiol-Lung Cell Mol. Physiol.* 289, 698 (2005).
131. A. A. Shvedova, E. R. Kisin, R. Mercer, A. R. Murray, V. J. Johnson, A. I. Potapovich, et al., *Am. J. Physiol. Lung Cell Mol. Physiol.* 289, L 698 (2005).